

Gravitational wave constraints on the shape of neutron stars

Nathan K. Johnson-McDaniel

Theoretisch-Physikalisches Institut, Friedrich-Schiller-Universität, Max-Wien-Platz 1, 07743 Jena, Germany

(Dated: June 5, 2018)

We show that there is a direct relation between upper limits on (or potential future measurements of) the $m = 2$ quadrupole moments of slowly rotating neutron stars and the $l = m = 2$ deformation of the star's surface, in full general relativity, to first order in the perturbation. This relation only depends on the star's structure through its mass and radius. All one has to assume about the star's constituents is that the stress-energy tensor at its surface is that of a perfect fluid, which will be true with good accuracy in almost all the situations of interest, and that the magnetic field configuration there is force-free, which is likely to be a good approximation. We then apply this relation to the stars which have direct LIGO/Virgo bounds on their $m = 2$ quadrupole moment, below the spin-down limit, and compare with the expected surface deformation due to rotation. In particular, we find that LIGO observations have constrained the Crab pulsar's $l = m = 2$ surface deformation to be smaller than its $l = 2, m = 0$ deformation due to rotation, for all the causal equations of state we consider, a statement that could not have been made just using the upper bounds on the $l = m = 2$ deformation from electromagnetic observations.

PACS numbers: 04.30.Tv, 04.40.Dg, 97.60.Jd

I. INTRODUCTION

In the absence of significant internal stresses, objects bound by gravity are highly symmetric on large scales. Indeed, Lindblom and Masood-ul-Alam [1, 2] have shown that all static perfect fluid relativistic stars are spherical (with reasonable assumptions about the equation of state). And even if one includes rotation, then equilibrium states of fluid stars must have a high degree of symmetry, as shown by Lindblom [3]: They must be axisymmetric, if one takes dissipation into account, and must have reflection symmetry across the equator, at least in the Newtonian approximation (though this is conjectured to hold for relativistic stars, as well).

However, situations in which the internal stresses are nonnegligible are not uncommon. Indeed, it is obvious that many of the smaller (though still gravitationally bound) objects in the solar system have large-scale internal stresses that are comparable to their self-gravity. This is particularly true for asteroids and the smaller moons, which can be highly nonspherical (see, e.g., [4] and Fig. 2.2 in [5]), but is even true for the larger moons and the terrestrial planets, to a less immediately apparent degree. (For instance, see the model for the Earth's gravitational field given in [6].) What is perhaps surprising is that such massive, strong-gravity objects as neutron stars can also have large enough internal stresses to produce a nonnegligible large-scale deformation, with reasonable theoretical input. In particular, as first appreciated by Ruderman [7], the star's solid crust can support a large-scale deformation, while an internal magnetic field will necessarily deform the star, as was first noted by Chandrasekhar and Fermi [8].

In most cases, these deformations will be quite small (maximum fractional deformations of $\sim 10^{-5}$, with considerably smaller deformations in most realistic cases). But there are certain scenarios in which the deforma-

tion could be (relatively) substantial ($\gtrsim 10^{-4}$, possibly as much as tens of percent in extreme cases): If there is a solid exotic phase (e.g., the hadron-quark mixed phase) in the star's core, the entire star is solid (as is the case for crystalline superconducting quark stars), or there is a large internal magnetic field of $\gtrsim 10^{15}$ G. (See, e.g., [9, 10] for the solid case and [11–14] for the magnetic case.)

The mechanisms for creating large deformations on nonaccreting neutron stars are not clear, though it is worth pointing out that neutron stars are expected to be born with some deformation from the violent supernova explosion that forms them, and it is possible that this deformation may be frozen in to the solid parts, and only relax slowly over time, as discussed in [15]. See also Sec. 2.2 in [16] for a discussion of scenarios involving accretion. However, deformed neutron stars are an interesting enough prospect for gravitational wave detection that it is worthwhile to consider the more extreme cases, and see what bounds there are on large deformations. In most cases, the best bounds on the large-scale deformations of neutron stars come from electromagnetic observations of their spin-down, which (as discussed in, e.g., [17]) constrain the star's $m = 2$ quadrupole moment, albeit with a factor of ~ 2 uncertainty due to the star's unknown moment of inertia. There are also tighter, though less direct, bounds that can be obtained from electromagnetic observations by folding in the star's braking index [18].

But the cleanest bounds come from gravitational wave observations, and a prominent accomplishment of the first generation of large-scale laser interferometer gravitational wave detectors has been setting direct upper bounds on the $m = 2$ quadrupole moment of certain known neutron stars, below the bounds that are given by electromagnetic observations of the spin-down, or indirect limits given by the star's age [15, 19–21]. See [16, 22, 23] for recent reviews. It is customary to quote these upper bounds in terms of a fiducial elliptic-

ity for the star to give a feeling for the size of the deformation. However, this fiducial ellipticity only gives a direct measure of the star’s deformation in the uniform density, Newtonian limit, and it is *a priori* unclear how to relate this to a measure of the deformation in more realistic cases. It is our purpose here to show how one can convert such fiducial ellipticities into a more physically meaningful, fully relativistic measure of the shape of the star’s surface. This relativistic shape measure gives a more tangible interpretation of present upper bounds on the gravitational radiation emitted from known pulsars than does the fiducial ellipticity. In particular, it allows one to compare the bounds on the star’s $l = m = 2$ deformation directly with various other deformations (e.g., the star’s deformation due to rotation, or the deformations of other astronomical objects). [*Nota bene* (N.B.): While there is also the possibility of an $m = 1$ quadrupole deformation, as discussed by Jones [24], we will not consider this situation here, since there are no final results for searches for such radiation—though see [25] for preliminary results. Similarly, we do not consider radiation from higher multipole deformations, as such radiation is suppressed by factors of the star’s rotational speed over the speed of light compared to the $l = 2$ radiation, and thus not searched for.]

The relativistic shape measure we define is inspired by the measure of the horizon deformation of a tidally distorted black hole used by Taylor and Poisson [26] and involves the ratio of the star’s longest polar circumference to its equatorial circumference. (Similar ratios have also been used in numerical studies of distorted black holes [27–29].) The conversion from fiducial ellipticity to relativistic shape measure only depends upon the star’s structure through its mass and radius (with reasonable assumptions about the magnetic field and shear stresses at the star’s surface). This simple conversion comes from the simple relation between the metric on the star’s perturbed surface and the surface value of the time-time component of the Regge-Wheeler gauge [30] metric perturbation (given by Damour and Nagar [31]), and the relationship between the surface value of this component and the amplitude of the star’s quadrupole gravitational radiation, given in [10] (the relation with the quadrupole moment was first given by Hinderer [32]). (As discussed in [10], these relations assume slow rotation, using the results of Ipser [33] and Thorne [34] to show that it is appropriate to calculate the gravitational waves from the rotating star using the quadrupole moment calculated in the static limit. This is quite a good approximation for the stars we consider, which are rotating well below the Kepler limit—at most $\sim 10\%$ of it.)

One can compute the deformation of the star due to rotation in the same manner, using Hartle’s classic calculation [35] of the metric of a slowly rotating relativistic star. While there is no reason to assume any sort of correlation between a star’s $l = m = 2$ deformation and its

rotational deformation,¹ the rotational deformation gives a convenient scale against which to compare the bounds on the $l = m = 2$ deformation. We then give these conversions (from fiducial ellipticity and rotational frequency to surface deformation) for a variety of equations of state (EOSs), including the case of a strange quark star (for which one needs to modify the calculations slightly). We also compare the bounds on the $l = m = 2$ surface deformation with the surface deformation due to rotation for the four stars with known spin periods for which the LIGO/Virgo bounds on the $l = m = 2$ deformation are near or below the (fiducial) spin-down limit. (We also note that models of strange quark stars with large radii can give significantly larger moments of inertia than the maximum of 3×10^{45} g cm² assumed in the LIGO/Virgo papers, which increases the uncertainty on the spin-down limit.) Additionally, we show that these results will receive negligible corrections from non-perfect fluid contributions in the cases of interest (with the possible exception of corrections to the force-free nature of the magnetic field configuration, which could be large enough to affect the results).

The paper is structured as follows: We define the shape measure, give some intuition about its properties, and detail how to compute it from the fiducial ellipticity in Sec. II. We then compute the surface deformation due to rotation in Sec. III, and compare the sizes of these two deformations for a variety of equations of state and pulsars of interest in Sec. IV. Finally, we conclude and consider the outlook for future bounds on the $l = m = 2$ deformations of known neutron stars in Sec. V. In the Appendix, we show that the corrections to these results due to the non-perfect fluid nature of real neutron stars are likely negligible in realistic cases. We use geometrized units throughout (i.e., take $G = c = 1$, where G is Newton’s gravitational constant and c is the speed of light).

II. THE RELATIVISTIC SHAPE MEASURE

A. Definition

First, recall that the fiducial ellipticity is defined by

$$\epsilon_{\text{fid}, 22} := \frac{I_{xx} - I_{yy}}{I_{zz}^{\text{fid}}}, \quad (1)$$

where I_{xx} and I_{yy} are the star’s *actual* moments of inertia about the axes other than its rotation axis (the difference between the two is related to the star’s $m = 2$ quadrupole moment, which is the observable quantity)

¹ Indeed, millisecond pulsars, which have the largest rotational deformations, for a fixed mass, have some of the tightest spin-down constraints on their $m = 2$ quadrupoles—see, e.g., Table 1 in [15]; one can obtain a star’s spin-down ellipticity by dividing the ellipticity bound given in the table by the value of $h_0^{95\%}/h_0^{\text{sd}}$.

and $I_{zz}^{\text{fid}} = 10^{45}$ g cm² is the *fiducial* moment of inertia of the star about its rotational axis. [As is discussed in, e.g., Sec. VI B of [17], the actual moment of inertia of neutron stars is expected to lie in the range $(1-3) \times 10^{45}$ g cm², on theoretical grounds, but there are no measurements of this quantity for any neutron star. And as we shall see, one can obtain even larger moments of inertia, up to at least $\sim 5.5 \times 10^{45}$ g cm², for models of strange quark stars with large radii.]

In contrast, our relativistic measure of the deformation will be constructed solely from quantities on the star's surface, which could be measured (in principle) by a physical observer, viz., the star's equatorial circumference, $s_{\text{eq}, 22}$, and its longest polar circumference, $s_{\text{pol}, 22, \text{max}}$, giving

$$\epsilon_{\text{surf}, 22} := \frac{s_{\text{pol}, 22, \text{max}} - s_{\text{eq}, 22}}{s_{\text{eq}, 22}} \quad (2)$$

(cf. the calculation of the surface deformation of a tidally deformed black hole in Sec. VIII of Taylor and Poisson [26], and the calculations of the shape of deformed black holes in [27–29]).² One can compute the quantities entering this definition using the metric on the star's surface, so all we need to do is write this metric in terms of the star's quadrupole moment (along with its unperturbed mass and radius).

To gain some intuition about the properties of this deformation measure, we consider a Newtonian ellipsoid, with semi-axes $(1 + \eta)R$, $(1 - \eta)R$, and R , for which we have $\epsilon_{\text{surf}, 22} = \eta/2$ (to first order in η). [Here we have used the expression $2\pi a[1 - e^2/4 + O(e^4)]$ for the circumference of an ellipse with semi-major and semi-minor axes a and b and eccentricity $e = \sqrt{1 - b^2/a^2}$.] If the ellipsoid has uniform density, then $I_{xx} - I_{yy} = 4\eta I_{zz} = (8/5)\eta MR^2$ [note that here we are using the *true* moment of inertia about the z -axis, $I_{zz} = (2/5)MR^2$, not the fiducial one, here and still working to first order in η], so its Newtonian ellipticity is $\epsilon_{N, 22} = 4\eta$, giving $\epsilon_{\text{surf}, 22} = \epsilon_{N, 22}/8$.

B. Computation

Let us now relate the relativistic shape measure to the star's fiducial ellipticity. The star's surface metric is given in standard spherical coordinates by Eqs. (85) and (86) in Damour and Nagar [31]

$$ds^2 = R^2 \left(1 + 2\frac{\delta R}{R} Y_{lm} \right) (d\theta^2 + \sin^2\theta d\phi^2), \quad (3)$$

where R is the star's undeformed radius, Y_{lm} is a spherical harmonic (we shall only consider $l = m = 2$ in our

discussion), and the deformation is given by [Eqs. (90) and (92) in Damour and Nagar [31]]

$$\frac{\delta R}{R} = -\frac{1}{2}H_0(R) \left[\frac{2}{\mathcal{C}} - 1 + \frac{\mathcal{C}}{2} + \frac{\mathcal{C}^2/4}{1-\mathcal{C}} + \frac{\mathcal{C}}{4} \frac{d \log H_0(R)}{d \log R} \right]. \quad (4)$$

Here $H_0(R)$ is the surface value of the time-time component of the $l = m = 2$ piece of the Regge-Wheeler gauge [30] perturbation of the star's metric [see Eq. (24) in [10] for the full perturbed metric, which comes from the stellar perturbation formalism of Thorne and Campolattaro [36]] and $\mathcal{C} := 2M/R$ is the star's compactness, where M is the star's mass. (Note that Damour and Nagar denote our H_0 by merely H and define a compactness of half our \mathcal{C} , which they denote by c .) This expression assumes a nonrotating star, but this is quite a good approximation for the stars in question, since they are rotating slowly enough that one can also treat their rotation as a perturbation of a static star, and the two perturbations are independent to first order (since their multipolar structure is different). The corrections due to rotation will thus be at most $\sim 1\%$. Additionally, as discussed in [10], the gravitational quadrupole radiation from a slowly rotating star can be computed from the static quadrupole moment of the star with no rotation, as shown by Ipser [33] and Thorne [34].

We now want to relate this to the $m = 2$ quadrupole moment of the deformed star. Here we consider the quadrupole moment amplitude Q_{22} given by

$$Q_{22} = \int_0^\infty \delta\rho(r)r^4 dr \quad (5)$$

in the Newtonian limit (the relativistic version is read off of the asymptotic expansion of the metric). (Here $\delta\rho$ is the $l = m = 2$ piece of the star's density perturbation.) We thus substitute the expression for $H_0(R)$ in terms of Q_{22} from Eqs. (39) and (41) in [10], giving

$$\begin{aligned} \frac{\delta R}{R} &= -\frac{1}{2} \frac{\pi Q_{22}}{M^3} \bar{H}_0(R) \left[\frac{2}{\mathcal{C}} - 1 + \frac{\mathcal{C}}{2} + \frac{\mathcal{C}^2/4}{1-\mathcal{C}} \right. \\ &\quad \left. + \frac{\mathcal{C}}{4} \frac{d \log \bar{H}_0(R)}{d \log R} \right] \\ &=: -\frac{1}{2} \frac{\pi Q_{22}}{M^3} \bar{f}_{22}(\mathcal{C}). \end{aligned} \quad (6)$$

Here we have defined $\bar{H}_0(R)$ to stand for $H_0(R)$ with unit amplitude (i.e., $c_1 \rightarrow 1$), so

$$\begin{aligned} \bar{H}_0(R) &= \left(\frac{2}{\mathcal{C}} - 1 \right) \frac{\mathcal{C}^2/2 + 3\mathcal{C} - 3}{1-\mathcal{C}} + \frac{6}{\mathcal{C}} \left(1 - \frac{1}{\mathcal{C}} \right) \\ &\quad \times \log(1-\mathcal{C}), \end{aligned} \quad (7)$$

and have also defined the “correction factor” $\bar{f}_{22}(\mathcal{C})$. [Since $\bar{H}_0(R)$ only depends on \mathcal{C} , the correction factor indeed only depends on \mathcal{C} . Also note that $d \log \bar{H}_0(R)/d \log R = -d \log \bar{H}_0(R)/d \log \mathcal{C}$.]

It is necessary to make a small change to the computation of $\delta R/R$ to treat the case of strange quark stars,

² Note that in the rotational case, these circumferences can no longer be determined directly from timelike or null geodesics, due to frame dragging.

where the density does not go to zero at the surface. This affects the present calculation because the pressure perturbation no longer goes to zero at the surface, so one must add on $\pi H_0(R)R^2\rho_-$ to the expression for $\delta R/R$ given in Eq. (4), where ρ_- is the density just inside the star's surface. This addition comes from noting that [Eqs. (88) and (91) in Damour and Nagar [31], recalling that their K is the negative of ours]

$$\frac{\delta R}{R} = \left[\left(1 - \frac{1}{\mathcal{C}}\right) H_0 + \frac{K}{2} \right] \Big|_{r=R}, \quad (8)$$

so we need to take into account corrections to the relation between K and H_0 from the nonzero surface density. Such corrections can be read off from Eq. (39a) in Ipser [33], which gives an addition to K of $-4\pi R^2\delta p$ at the surface, where δp is the $l = m = 2$ piece of the Eulerian pressure perturbation, and is denoted $-p_1$ by Ipser. We then use the stress-energy conservation expression for δp given in Eq. (35) of [10] to obtain $\delta p = -H_0(R)\rho_-/2$ at the surface, which then yields the expression given above. [N.B.: We neglect the shear stress terms in all of these relations, which we shall show is a good approximation in the Appendix.] However, this contribution only decreases the star's deformation by $\lesssim 5\%$ in the case we consider.

We now compute the desired arclengths, finding (to first order in $\delta R/R$)

$$s_{\text{eq}, 22} = R \int_0^{2\pi} \left[1 + \sqrt{\frac{15}{32\pi}} \frac{\delta R}{R} \cos 2\phi \right] d\phi = 2\pi R \quad (9)$$

and

$$\begin{aligned} s_{\text{pol}, 22} &= 2R \int_0^\pi \left[1 + \sqrt{\frac{15}{32\pi}} \frac{\delta R}{R} \sin^2 \theta \cos 2\phi_0 \right] d\theta \\ &= 2\pi R \left[1 + \sqrt{\frac{15}{128\pi}} \frac{\delta R}{R} \cos 2\phi_0 \right], \end{aligned} \quad (10)$$

where we have used $\text{Re } Y_{22} = \sqrt{15/32\pi} \sin^2 \theta \cos 2\phi$ and considered the longitude line with azimuthal angle ϕ_0 . We can now write $\epsilon_{\text{surf}, 22}$ in terms of Q_{22} , or the fiducial $l = m = 2$ ellipticity $\epsilon_{\text{fid}, 22} = \sqrt{8\pi/15} Q_{22}/I_{zz}^{\text{fid}}$, using Eqs. (2) and (6), yielding

$$\begin{aligned} \epsilon_{\text{surf}, 22} &= \sqrt{\frac{15\pi}{512}} \frac{Q_{22}}{M^3} \bar{f}_{22}(\mathcal{C}) = \frac{15}{64} \frac{I_{zz}^{\text{fid}}}{M^3} \bar{f}_{22}(\mathcal{C}) \epsilon_{\text{fid}, 22} \\ &=: f_{22}(M, \mathcal{C}) \epsilon_{\text{fid}, 22}. \end{aligned} \quad (11)$$

Here $f_{22}(M, \mathcal{C})$ gives the conversion factor between the ($l = m = 2$) fiducial ellipticity and the $l = m = 2$ surface deformation. [N.B.: Since $\bar{f}_{22}(\mathcal{C}) > 0$, we have $\delta R/R < 0$, and thus the maximum value of $s_{\text{pol}, 22}$ is given by taking $\cos 2\phi_0 = -1$.]

Note that in the Newtonian limit, we have $\epsilon_{\text{surf}, 22} = (3/8)(I_{zz}^{\text{fid}}/MR^2)\epsilon_{\text{fid}, 22}$. This does not agree with the Newtonian calculation for the uniform density ellipsoid given at the end of Sec. II A, which gives a coefficient of

5/16, but that is to be expected, since the present computation assumes a fluid star, whose surface will deform to be an equipotential of its perturbed gravitational field, while the ellipsoid was taken to be rigid.

III. CALCULATION OF THE ROTATIONAL DEFORMATION

It is interesting to compare upper bounds on an $l = m = 2$ deformation to the $l = 2, m = 0$ deformation induced by the star's rotation. Here, one can use the slow-rotation results of Hartle [35] to perform the calculation. We start by recalling that [Eq. (86) in Damour and Nagar [31]; cf. Eq. (25a) in Hartle and Thorne [37]]

$$\frac{\delta R}{R} = \frac{\delta r}{r} + \frac{1}{2}K(R), \quad (12)$$

where $\delta r/r$ gives the fractional position of the star's deformed surface, and $K(R)$ is the ($l = 2, m = 0$ piece of the) angular component of the metric perturbation, evaluated at the star's surface.³ [Here, following Hartle, we take the angular dependence to be just the Legendre polynomial portion of Y_{20} , viz., $(3 \cos^2 \theta - 1)/2$, without the normalization factor of $\sqrt{5/4\pi}$ present in the spherical harmonic. Additionally, note that we have reversed the sign of Damour and Nagar's K to correspond to the conventions of Hartle [35] and [10].]

We will obtain expressions for the quantities entering Eq. (12) in terms of the surface values of Hartle's h_2 and k_2 , the $l = 2, m = 0$ components of the time-time and angular metric perturbations [see Eqs. (66)–(69) in Hartle [35]], noting that $K = 2k_2$ [cf. Hartle's Eq. (66) and Eq. (24) in [10]]. We will then solve the equations Hartle gives for h_2 and $v := h_2 + k_2$ to obtain these surface values for a given stellar model.

Specifically, to obtain $\delta r/r$, we note that Eq. (146) in Hartle [35] gives an expression for Hartle's ξ_2/a , which is the same as our $\delta r/r$, so we have

$$\frac{\delta r}{r} = \left(2 - \frac{2}{\mathcal{C}}\right) h_2(R) - \frac{8M^2}{3\mathcal{C}^3} \left(\Omega - \frac{J\mathcal{C}^3}{4M^3}\right)^2, \quad (13)$$

where

$$\begin{aligned} h_2(R) &= A \left[-\frac{6(1-\mathcal{C})}{\mathcal{C}^2} \log(1-\mathcal{C}) - \frac{6}{\mathcal{C}} + 3 + \mathcal{C} + \frac{\mathcal{C}^2/2}{1-\mathcal{C}} \right] \\ &\quad + \frac{J^2\mathcal{C}^3}{8M^4} \left(1 + \frac{\mathcal{C}}{2}\right) \end{aligned} \quad (14)$$

[Eqs. (137) and (139) in Hartle [35]], Ω is the magnitude of the star's angular velocity, and $J = I_{zz}\Omega$ is the magnitude of its angular momentum, where I_{zz} is the star's

³ We neglect the $l = 0$ change to the star's radius, since it gives a second-order correction to the calculation of the relativistic shape measure.

(true) moment of inertia. Here we have noted that Hartle's $\zeta := 2/\mathcal{C} - 1$. We obtain $K(R)$ from Eqs. (137) and (139)–(141) in Hartle [35], giving

$$\frac{1}{2}K(R) = A \left[\frac{6}{\mathcal{C}} + 3 - \mathcal{C} + 3 \left(\frac{2}{\mathcal{C}^2} - 1 \right) \log(1 - \mathcal{C}) \right] - \frac{J^2 \mathcal{C}^3}{8M^4} (1 + \mathcal{C}). \quad (15)$$

The amplitude A is given by solving [Eqs. (125) and (126) in Hartle [35]]

$$v' = -2\phi' h_2 + \frac{1}{6} (1 + r\phi') [r^3 j^2 (\bar{\omega}')^2 - 2r^2 (j^2)' \bar{\omega}^2], \quad (16a)$$

$$h_2' = \left\{ -2\phi' + \frac{r}{[r - 2m(r)]\phi'} \left[4\pi(\rho + p) - \frac{2m(r)}{r^3} \right] \right\} h_2 - \frac{2v}{r[r - 2m(r)]\phi'} + \frac{1}{6} \left\{ r\phi' - \frac{1}{2[r - 2m(r)]\phi'} \right\} \times r^3 j^2 (\bar{\omega}')^2 - \frac{1}{3} \left\{ r\phi' + \frac{1}{2[r - 2m(r)]\phi'} \right\} r^2 (j^2)' \bar{\omega}^2, \quad (16b)$$

where primes denote derivatives with respect to the (Schwarzschild) radial coordinate r ; ρ and p are the star's energy density and pressure, respectively; we have [cf. Eqs. (26)–(29) and (40) in Hartle [35]]

$$\phi' = \frac{m(r) + 4\pi r^3 p}{r[r - 2m(r)]}, \quad (17a)$$

$$\phi(R) = \log(1 - 2M/R)/2, \quad (17b)$$

$$m(r) := 4\pi \int_0^r \rho(\bar{r}) \bar{r}^2 d\bar{r}, \quad (17c)$$

$$j := \left[1 - \frac{2m(r)}{r} \right]^{1/2} e^{-\phi}; \quad (17d)$$

and the frame-drag parameter $\bar{\omega}$ is given by [Eq. (46) in Hartle [35]]

$$\frac{1}{r^4} (r^4 j \bar{\omega}')' + \frac{4}{r} j' \bar{\omega} = 0. \quad (18)$$

[Note that Hartle denotes 2ϕ by ν and $2\phi'$ by ν_R . We have chosen to use the same notation as in [10] to avoid confusion with our use of ν for the star's spin frequency here. Similarly, we use ρ and p for the star's energy density and pressure instead of Hartle's E and P . Finally, we generally suppress the arguments of functions when we are not evaluating them at a specific point, unless we feel that the argument needs to be included for clarity, as with $m(r)$.]

We slightly streamline the solution process for v and h_2 given above Hartle's Eq. (146): We still write the solution as a linear combination of the solutions to the homogeneous and inhomogeneous equations and determine the unknown coefficients by matching the solution

and its first derivative to the known exterior solutions at the surface of the star [Eqs. (14) and (15), recalling that $v = h_2 + K/2$]. However, we find that it is not necessary to use Hartle's more involved inner boundary conditions, and that we can simply integrate the inhomogeneous equations starting from values of 0 at r_0 , the inner radius where we impose our inner boundary condition when solving the enthalpy version of the Oppenheimer-Volkov equations [38]—see the discussion at the end of Sec. III in [10]. We also take boundary conditions for the homogeneous equations [i.e., Eqs. (16) with the source terms that do not contain v and h_2 omitted] of $h_2(r_0) = r_0^2/R^2$ and $v_2(r_0) = -2\pi(p_c + \rho_c/3)r_0^4/R^2$ [cf. Eqs. (128) and (144) in Hartle [35]]. Here p_c and ρ_c denote the central values of the pressure and energy density, which are the same as those at r_0 , in our treatment. The boundary condition for $\bar{\omega}$ is given by $\bar{\omega}(0) = \text{const}$; one then scales the final result to give the desired angular velocity, using the known solution of $\bar{\omega}(r) = \Omega - 2J/r^3$ outside the star [Eq. (47) in Hartle [35]], noting that the surface deformation scales as Ω^2 .

Additionally, we convert Eqs. (16) and (18) to enthalpy form (i.e., with the enthalpy h as the dependent variable; despite notation, this has no relation to h_2). This was first done for the frame-drag equation (18) in Sec. 4.1 of K. Lockitch's thesis [39]. [The transformed frame-drag equation also appears in a slightly different form in Appendix A of [40]. Since this transformation is simply performed by dividing through by $h'(r)$ and substituting $r \rightarrow r(h)$, we choose not to show the transformed equations explicitly.] Finally, we perform the matching at the surface using h_2 and its first derivative to obtain the amplitude A [cf. Eq. (14)], and use the v_2 matching as a check. (This check indicates that our calculations are accurate to better than $\sim 2\%$, usually much better.)

We must also consider the changes that need to be made to this calculation to treat strange quark stars, with their nonzero surface density. Due to Hartle's method of locating the surface of the rotating star using a first integral to the equations of hydrostatic equilibrium, no change is necessary in that portion of the calculation. However, we do need to modify the surface matching used to obtain the amplitude. The calculation of the moment of inertia remains unchanged, since only the second derivative of $\bar{\omega}$ is discontinuous at the surface. But the contribution to $(j^2)'$ from the density evaluated just inside the star's surface is $-8\pi R \rho_- / (1 - \mathcal{C})$ [from Eqs. (17), noting that $e^{-2\phi(R)} = 1/(1 - \mathcal{C})$]. Thus, the matching of the solutions to Eqs. (16) at the surface needs to be adjusted using the replacements

$$v'_{\text{out}} \rightarrow v'_{\text{out}} + \frac{4\pi}{3} \left(2 + \frac{\mathcal{C}}{1 - \mathcal{C}} \right) \frac{R^3 \rho_- \bar{\omega}^2(R)}{1 - \mathcal{C}}, \quad (19a)$$

$$h'_{2, \text{out}} \rightarrow h'_{2, \text{out}} + \frac{4\pi R^2 \rho_- h_2(R)}{M} + \frac{4\pi}{3} \left(\frac{2}{\mathcal{C}} + \frac{\mathcal{C}}{1 - \mathcal{C}} \right) \times \frac{R^3 \rho_- \bar{\omega}^2(R)}{1 - \mathcal{C}}, \quad (19b)$$

where the subscript “out” denotes the solution outside the star.

One can compare the values for the quadrupole obtained using the Hartle slow-rotation expansion with the fits to a fully relativistic calculation for a $1.4 M_\odot$ star given in Eq. (73) and Table 5 in Friebe and Rezzolla [13]. Here one uses Eq. (26) in [37] to obtain the quadrupole from the slow-rotation calculation (the expression given in [35] is in error). We find quite close agreement for the four EOSs we both consider—at worst, $\sim 2\%$ for the BBB2 and GNH3 EOSs, and at best, better than 0.1% , for the APR and SLy EOSs. (What we call the SLy EOS is the same as Friebe and Rezzolla’s SLy4; we give further discussion of these EOSs in Sec. IV.) Our calculations of the moment of inertia all agree to better than 0.1% .

Now doing the calculations of the equatorial and polar circumferences, we have, as previously,

$$\begin{aligned} s_{\text{eq}, 20} &= R \int_0^{2\pi} \left[1 - \frac{1}{2} \left(\frac{\delta R}{R} \right)_{20} \right] d\phi \\ &= 2\pi R \left[1 - \frac{1}{2} \left(\frac{\delta R}{R} \right)_{20} \right], \end{aligned} \quad (20)$$

$$\begin{aligned} s_{\text{pol}, 20} &= 2R \int_0^\pi \left[1 + \frac{1}{2} \left(\frac{\delta R}{R} \right)_{20} (3 \cos^2 \theta - 1) \right] d\theta \\ &= 2\pi R \left[1 + \frac{1}{4} \left(\frac{\delta R}{R} \right)_{20} \right], \end{aligned} \quad (21)$$

where $(\delta R/R)_{20}$ is calculated by combining together Eqs. (12)–(15). Thus, we have

$$\begin{aligned} \epsilon_{\text{surf}, 20} &:= \frac{s_{\text{eq}, 20} - s_{\text{pol}, 20}}{s_{\text{eq}, 20}} = -\frac{3}{4} \left(\frac{\delta R}{R} \right)_{20} \\ &=: g_{20}(M, \mathcal{C}) \nu^2 \end{aligned} \quad (22)$$

to first order in $\delta R/R$, where we have used the known scaling of the surface deformation with Ω^2 in the final equality to write $\epsilon_{\text{surf}, 20}$ in terms of the star’s spin frequency, ν , defining the conversion factor $g_{20}(M, \mathcal{C})$. We have also introduced a minus sign, compared with the $l = m = 2$ version, so that $\epsilon_{\text{surf}, 20}$ will be positive.

For the purposes of comparison, we relate our $\epsilon_{\text{surf}, 20}$ to the coordinate radius ellipticity or flattening in the Euclidean limit (and to first order in the deformation). This coordinate radius ellipticity is defined by

$$\epsilon_c = \frac{r_e - r_p}{r_e}, \quad (23)$$

where r_e and r_p are the star’s equatorial and polar radii, respectively, so we have $\epsilon_c = 2\epsilon_{\text{surf}, 20}$ in the given limit. (Here we have noted that the eccentricity of an ellipse is related to the flattening by $e^2 = 2\epsilon_c - \epsilon_c^2$. Note also that Friebe and Rezzolla [13] define their surface deformation to be $r_e/r_p - 1$ [see their Eq. (68)], though this agrees with ϵ_c to first order in the deformation.)

IV. RESULTS AND DISCUSSION

Here we show the results of our calculations for a representative selection of EOSs, whose mass-radius curves and moments of inertia versus mass are illustrated in Fig. 1. (All the calculations presented here were carried out using MATHEMATICA 7’s default methods.) Specifically, we have chosen the four EOSs from the LORENE library [41] that are compatible with the Demorest *et al.* [42] measurement of a $1.97 \pm 0.04 M_\odot$ neutron star (the nucleonic EOSs APR [43], BBB2 [44], and SLy [45] and the hyperonic EOS GNH3 [46]; note that BBB2 is only compatible within 2σ). We also consider the nucleonic WFF1 EOS [47], the most compact EOS considered in [40], obtained from the RNS website [48].⁴ For more exotic EOSs, we use three of the hadron-quark hybrid EOSs from [49] (Hy1, LKR1, and generic) and the strange quark matter EOS constructed in [10] using the results of Kurkela, Romatschke, and Vuorinen [50] (KRV1). Most of these EOSs are 1σ compatible with the very recent measurement of a $2.01 \pm 0.04 M_\odot$ neutron star by Antoniadis *et al.* [51].⁵ However, the GNH3 and LKR1 EOSs are only compatible within 2σ (though the GNH3 EOS is close to being 1σ compatible), while the BBB2 EOS is only compatible within 3σ . (The 3σ bounds are 1.90 and $2.18 M_\odot$.)

We show the conversion factor $f_{22}(M, \mathcal{C})$ for these EOSs in Fig. 2. Note also that if one considers a canonical $M = 1.4 M_\odot$, $R = 10$ km neutron star, then its compactness is ~ 0.42 , and $f_{22}(1.4 M_\odot, 0.42) \simeq 0.22$. Thus, we see that the fiducial ellipticity generally gives a reasonable impression of the size of the star’s surface deformation. Of course, the actual size of the deformation depends upon the star’s undeformed size: One can give a dimensionful measure of the surface deformation by multiplying ϵ_{surf} by the star’s radius, R (recalling that the star’s equatorial circumference is unchanged by the deformation, to linear order). We show this for the LIGO upper limits on the Crab’s quadrupole moment in Fig. 2, taking $\epsilon_{\text{fid}, 22} = 10^{-4}$ (around the best upper limit given in [15]). And while we have used the current upper limit on the Crab’s fiducial ellipticity, one can scale these results linearly to apply to any other fiducial ellipticity (for the Crab or any other neutron star).

Note, however, that if one considers elastic deforma-

⁴ Note, however, that the high compactness of stars obtained with the WFF1 EOS is in part attributable to the fact that this EOS becomes acausal (i.e., has a sound speed greater than the speed of light) at densities well below the central density of the maximum mass stable stars. The same is true for the EOS we consider that generates the second most compact stars, the APR EOS, which is computed using a variational method, like the WFF1 EOS. Thus, in our plots, we will mark the points at which stars constructed with these EOSs start to contain acausal matter.

⁵ But note that the Antoniadis *et al.* measurement relies on some modeling of white dwarf atmospheres, and is thus not as clean as the Demorest *et al.* [42] measurement considered above.

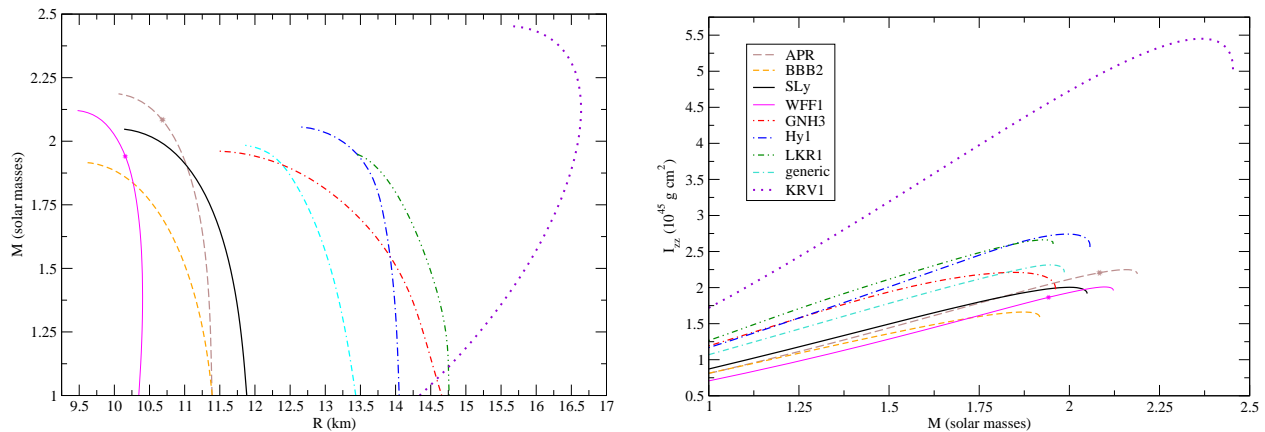


FIG. 1: The mass-radius relation (*left*) and moment of inertia versus mass (*right*) for the EOSs considered in this paper. For the APR and WFF EOSs, the asterisks mark the maximum mass for which the stars do not contain any acausal matter (i.e., for which the central density is smaller than the density at which the EOS has a sound speed greater than the speed of light).

tions, then the SLy EOS would not be able to support a quadrupole large enough to create a fiducial ellipticity anywhere close to 10^{-4} , unless one assumes a very low-mass star—see Figs. 5 and 6 in [10] and Fig. 3 in Horowitz [52]. This is simply because the crust is the only solid portion of neutron stars with nucleonic EOSs, like the SLy EOS (and even hyperonic EOSs), and the crustal shear modulus is (relatively) small, compared with the shear moduli of the higher-density solids that may be present in more exotic EOSs. Thus, while there do not yet exist calculations for the maximum deformations that could be sustained by the other hadronic or hyperonic EOSs, they also should not be able to support such large quadrupoles, with standard crustal compositions, since stars constructed with these EOSs have compactnesses that are roughly the same as those obtained using the SLy EOS. And even the three hybrid EOSs shown would only be able to support a quadrupole large enough to create such a large fiducial ellipticity for high masses—see Fig. 9 in [10]. However, as shown in Fig. 10 in [10], one could easily obtain such a large quadrupole with the KRV1 EOS, assuming that the strange matter is in a crystalline state, with a shear modulus given by the Mannarelli, Rajagopal, and Sharma [53] calculation, and that its breaking strain is $\sim 10^{-1}$, similar to that obtained for the neutron star outer crust in [54, 55].⁶ And strong enough internal magnetic fields could sustain such a large quadrupole for all EOSs. See, in particular, the calculations of magnetic deformations by Friebe and Rezzolla [13] for four of the nucleonic EOSs we consider.

Now considering the rotational deformations, we show the conversion factor $g_{20}(M, C)$ and the dimensionful sur-

face deformation for the Crab in Fig. 2. Again, one can scale the results for the Crab to any other (slowly rotating) pulsar, using the scaling of the surface deformation with ν^2 .

The behavior of all these quantities is as expected: As the star becomes more massive and more compact, one finds that a given $m = 2$ quadrupole moment (i.e., a given fiducial $l = m = 2$ ellipticity) translates into a smaller surface deformation, as one would anticipate, since the star’s moment of inertia is increasing. This trend reverses for the highest masses, however, where the relativistic suppressions of the quadrupole due to the increasing compactness (discussed in Sec. V of [10]) now dominate. Additionally, the more massive, compact stars do not deform as easily, and this is seen in the mass dependence of the rotational deformation. In the strange quark star case, one even sees that the decrease in deformability with increasing mass is strong enough to dominate the increase in radius. In general, for a fixed rotation rate and fiducial ellipticity, the $l = m = 2$ surface deformation is the largest and the rotational deformation is the smallest for the most compact stars. This is illustrated using the bounds and expectations for the dimensionful surface deformation of the Crab pulsar and the most compact EOSs we consider (all nucleonic) in Fig. 3.

In Table I, we compare the LIGO/Virgo upper bounds on the $l = m = 2$ deformation with the expected rotational deformations for the four neutron stars for which the LIGO/Virgo bounds are lower than indirect limits, and there is a measured spin period (viz., the Crab and Vela pulsars, J0537–6910, and J1952+3252) [15, 21]. We do this assuming the fiducial $1.4 M_\odot$ neutron star and considering all the EOSs used in this paper. But recall that there is no reason to assume any correlation between the $l = m = 2$ and $l = 2, m = 0$ deformations. We merely quote the numbers for rotation as a convenient scale against which to compare the upper bounds on the nonaxisymmetric deformations.

⁶ As discussed in [10], the large breaking strain found for the neutron star outer crust is due to its high pressure, so it is reasonable to expect that the breaking strain of other materials under similar or greater pressures to be comparable.

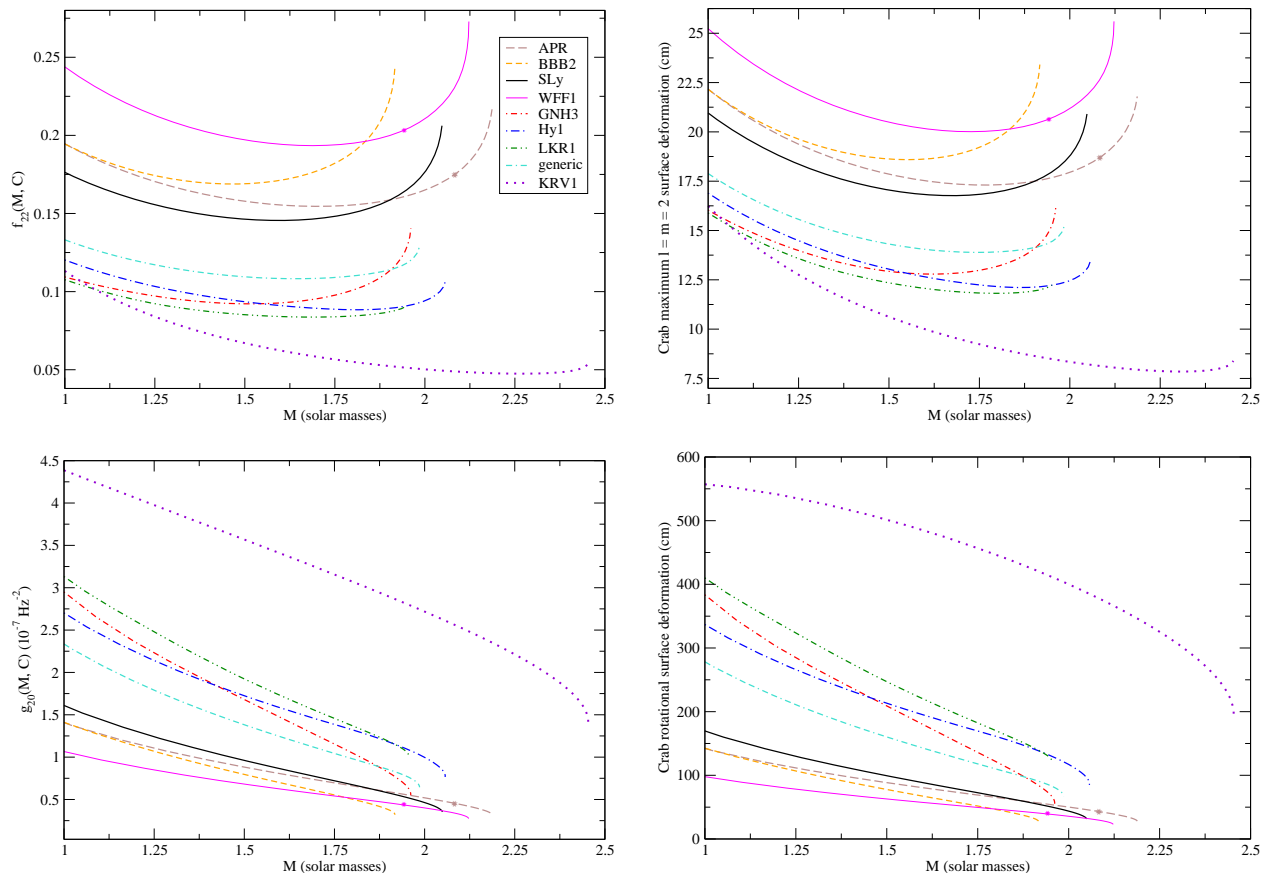


FIG. 2: The $l = m = 2$ (upper left) and rotational (lower left) conversion functions [$f_{22}(M, C)$ and $g_{20}(M, C)$] and the maximum $l = m = 2$ (upper right) and expected rotational (lower right) surface deformations for the Crab pulsar in dimensionful form (i.e., $R\epsilon_{\text{surf}, 22}$ and $R\epsilon_{\text{surf}, 20}$), all versus mass and for the various EOSs we consider. For the maximum $l = m = 2$ Crab pulsar surface deformations, we use the LIGO upper bound on the fiducial ellipticity of $\epsilon_{\text{fid}, 22}^{\text{max}} = 10^{-4}$. Also, for the APR and WFF1 EOSs, the asterisks mark the maximum masses that do not contain acausal matter.

Additionally, note that the last two stars we consider require a moment of inertia larger than the fiducial one (of 10^{45} g cm^2), or a significantly closer distance than the estimate used in [15] in order for the LIGO upper bound to beat the spin-down limit. This is not too much of a concern for J0537–6910, as one only needs a factor of ~ 2 larger moment of inertia, which is easily provided by any number of EOSs (see, e.g., this paper’s Fig. 1 and Fig. 6 in [57]). However, for J1952+3252, [15] claims that LIGO likely just misses beating the spin-down limit, even given the uncertainties in distance and moment of inertia. We have still included this star here, since the requisite moment of inertia of $\gtrsim 4 \times 10^{45} \text{ g cm}^2$ would be easily attainable with the KRV1 EOS for higher masses.⁷

Additionally, there is a fair amount of uncertainty in this pulsar’s distance: Using H I measurements, Verbiest *et al.* [58] give distance bounds of $3 \pm 2 \text{ kpc}$, so on the small side, this is significantly closer than the distance of 2.5 kpc used in [15], and would be enough to put the LIGO bound under the spin-down limit, even assuming the fiducial moment of inertia. (However, note that reducing the distance would reduce the inferred limit on the fiducial ellipticity from the LIGO results, in addition to increasing the spin-down limit, while increasing the moment of inertia does not affect the limit on the fiducial ellipticity.) But even these large strange quark star moments of inertia are not quite large enough to make the LIGO limit lie below a reasonable spin-down limit for J1913+1011, the pulsar with the next closest LIGO limit to its fiducial spin-down limit, without assuming that the pulsar is significantly closer than thought: The

⁷ In considering the effects of the moment of inertia on the spin-down limit, be aware of the following typographical errors in [15]: In that paper’s Eqs. (1) and (7), I_{38} should be $I_{38}^{1/2}$ and I_{38}^{-1} , respectively. The first of these errors is also present in an inline equation in the first paragraph of Sec. 1 of [19] and Eq. (14) of [21] [though Eq. (1.2) in [17] is correct]. The second is also present

in the first paragraph of Sec. 3 of [19], though the analogous Eqs. (6.1) in [17] and (15) in [21] are correct.

	Crab		Vela		J0537–6910		J1952+3252	
ν (Hz)	29.8		11.2		62.0		25.3	
$\epsilon_{\text{fid}, 22}^{\text{max}}$	1.0×10^{-4}		1.1×10^{-3}		1.0×10^{-4}		2.3×10^{-4}	
(10^{-5})	$\epsilon_{\text{surf}, 22}$	$\epsilon_{\text{surf}, 20}$						
(cm)	$R\epsilon_{\text{surf}, 22}$	$R\epsilon_{\text{surf}, 20}$						
APR	1.6	8.6	18	1.2	1.6	37	3.7	6.2
	18	97	200	14	18	420	42	70
BBB2	1.7	8.0	19	1.1	1.7	35	3.9	5.8
	19	89	210	13	19	390	43	64
SLy	1.5	9.5	16	1.3	1.5	41	3.4	6.8
	17	110	190	16	17	480	40	80
WFF1	2.0	6.6	22	0.93	2.0	29	4.6	4.8
	21	69	230	9.7	21	300	48	50
GNH3	0.93	17	10	2.4	0.93	73	2.1	12
	13	240	150	34	13	1000	30	170
Hy1	0.97	17	11	2.4	0.97	72	2.2	12
	14	230	150	33	14	1000	31	170
LKR1	0.87	19	9.6	2.7	0.87	82	2.0	14
	13	280	140	39	13	1200	29	200
generic	1.1	14	12	1.9	1.1	59	2.6	9.8
	15	180	160	25	15	780	34	130
KRV1	0.73	33	8	4.7	0.73	140	1.7	24
	11	520	120	73	11	2200	26	370

TABLE I: The maximum $l = m = 2$ and expected rotational ($l = 2, m = 0$) surface deformations (both dimensionless and dimensional) for the four pulsars for which there are LIGO/Virgo upper bounds below the spin-down limit, for the various EOSs we consider, assuming a $1.4 M_{\odot}$ star. We also give the stars’ rotational frequencies ν , and the upper bounds on fiducial ellipticity from the LIGO/Virgo results, $\epsilon_{\text{fid}, 22}^{\text{max}}$. The values for ν are valid for the years 2005–2007, corresponding to the time of the gravitational wave observations. The Vela pulsar observations were later, but the Vela pulsar’s spin-down is relatively slow, so its spin frequency is not affected, to the given accuracy. Indeed, the spin frequencies given are the same as the current ones to the given accuracy for all pulsars except for the Crab: The Crab pulsar spins down rather rapidly, so its current spin frequency is 29.7 Hz (from the Jodrell Bank Crab Pulsar Monthly Ephemeris [56]), which reduces its rotational surface deformation by $\sim 0.7\%$ compared with the values given in the table. All values for the deformations are rounded to two significant figures.

LIGO limit for J1913+1011 is 4.9 times its fiducial spin-down limit, and the spin-down limit scales as $I_{zz}^{1/2}$ —cf. Eq. (1.2) in [17].

Considering the EOSs presented here, we can see that gravitational wave observations have constrained the large-scale (i.e., $l = 2$) surface deformation on the Crab to be due to rotation, not to any sort of $l = m = 2$ distortion. [The only exception comes from the near-maximum mass stars given by the WFF1 EOS, with its high maximum compactness of 0.668; note that such stars contain a significant region ($\sim 15\%$ by volume) of acausal matter.] This conclusion could *not* have been made solely from electromagnetic observations, since the star’s spin-down only puts a limit on the $l = m = 2$ deformation that is at least ~ 7 times greater than the LIGO limit (and possibly a factor of a few more, given the uncertainties in the moment of inertia)—see Table 3 in [15]. This would only be sufficient to constrain the Crab pulsar’s $l = m = 2$ surface deformation to be smaller than its rotational surface deformation for stars with large radii. (Note that some interpretations of X-ray observations of neutron stars [59, 60] imply that their radii are ~ 11 – 12 km, so the EOSs that give stars with larger radii may be disfavored, though these interpretations are by no means conclusive.) And even the smaller, less direct

upper limit obtained by Palomba [18] by folding in the star’s braking index only bounds the deformation to be ~ 3 times larger than the LIGO bound, which would be insufficient to ensure that the $l = m = 2$ surface deformation is smaller than the rotational surface deformation for massive, compact stars, as shown in Fig. 3. (While we have used the best upper limit for the Crab’s fiducial ellipticity given in Table 3 in [15] in drawing this conclusion, note that improved bounds from LIGO/Virgo are forthcoming [25], so this is a mild caveat.)

Since the Vela pulsar spins at less than half the frequency of the Crab pulsar, and has an upper bound on its fiducial ellipticity that is an order of magnitude greater, the observations do not bound its $l = m = 2$ surface deformation to be smaller than its rotational surface deformation, even for the case in which the two deformations are the most similar, the LKR1 EOS and a mass of $\sim 1.8 M_{\odot}$. Conversely, since J0537–6910 has a rotational frequency that is ~ 2 times the Crab’s and the same bound on its fiducial ellipticity, we know that its rotational deformation is larger than its $l = m = 2$ deformation for all masses and EOSs, even for the most massive, compact stars with the WFF1 EOS. (Indeed, the spin is large enough that this conclusion could have been obtained from the electromagnetic observations of

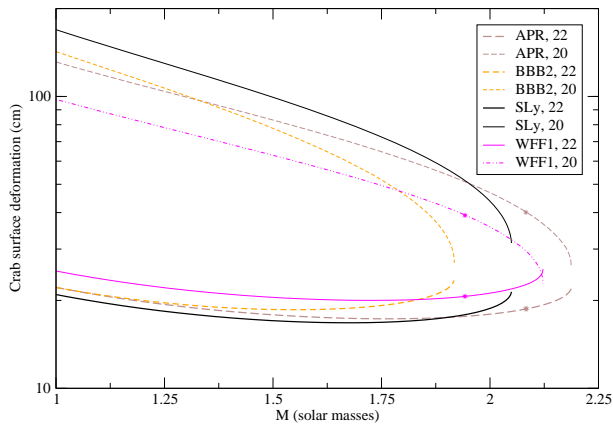


FIG. 3: The maximum $l = m = 2$ (lower curves) and expected rotational ($l = 2, m = 0$; upper curves) dimensionful deformations (i.e., $R\epsilon_{\text{surf}, 22}$ and $R\epsilon_{\text{surf}, 20}$) of the Crab pulsar versus mass for the hadronic EOSs we consider, using the LIGO bound of $\epsilon_{\text{fid}, 22}^{\text{max}} = 10^{-4}$. As before, asterisks denote the maximum masses that do not contain acausal matter for the APR and WFF1 EOSs.

the spin-down, even with the uncertainties in the moment of inertia.) The bounds on J1952+3252’s $l = m = 2$ surface deformation compared with its rotational deformation are similar to the Crab’s, though somewhat less good, due to J1952+3252’s somewhat smaller spin frequency and the larger upper bound on its fiducial ellipticity. In particular, the bound on J1952+3252’s $l = m = 2$ surface deformation will be larger than its rotational surface deformation for masses slightly larger than $1.4 M_{\odot}$ for the WFF1 EOS, and for all the other nucleonic EOSs for larger masses.

Finally, for a close-to-home scale against which to compare these surface deformations, the Earth’s (dimensionless) rotational surface deformation is $\sim 1.7 \times 10^{-3}$, and the (dimensionless) $l = m = 2$ surface deformation of the geoid (i.e., of a gravitational equipotential near sea level) is $\sim 2.8 \times 10^{-6}$. These values were obtained using the value of the flattening of the Earth’s reference ellipsoid and the $l = m = 2$ component of the Earth’s gravitational field, both from the WGS84 version of the Earth Gravitational Model EGM2008 [6], along with the relation between the flattening and the rotational surface deformation given at the end of Sec. III. The Crab pulsar’s and J1952+3252’s (dimensionless) rotational surface deformations are thus very similar to the Earth’s for the EOSs with larger radii, if the pulsars’ masses are close to $1.4 M_{\odot}$. However, all of the bounds on the $l = m = 2$ (dimensionless) surface deformation for the pulsars we consider are larger than the Earth’s $l = m = 2$ (dimensionless) surface deformation, though the bounds (electromagnetic or gravitational wave) for many of the faster rotating pulsars are well below this (see Table 1 in [15]).

V. CONCLUSIONS AND OUTLOOK

We have shown that one can convert the bounds on the fiducial ellipticity of neutron stars (from gravitational wave or electromagnetic observations) into bounds on the shape of the star’s surface, in full general relativity, to first order in the perturbation (and in the slow-rotation limit). We have given the conversion for a variety of EOSs, some purely nucleonic and others containing exotica, including the strange quark star case (with the requisite changes to the calculation), and compared with the shape of the star’s surface due to rotation. Here we find that the gravitational wave observations have constrained the Crab pulsar’s $l = m = 2$ surface deformation to be smaller than its $l = 2, m = 0$ surface deformation due to rotation, for all the causal EOSs we consider.

For the other three pulsars for which LIGO/Virgo observations have beaten the spin-down limit, within the uncertainties on the star’s distance and moment of inertia, we find that the Vela pulsar’s relatively slow rotation means that the bound on its $l = m = 2$ surface deformation is well above its rotational surface deformation, for all the EOSs we consider. On the other hand, for the more quickly rotating J0537–6910, the $l = m = 2$ surface deformation is known to be below the rotational deformation from the electromagnetic observations of its spin-down. (Again, this holds for all the EOSs we consider.) For J1952+3252, the bound on the $l = m = 2$ surface deformation is below the rotational surface deformation for all cases except for heavy stars constructed with the hadronic EOSs.

Looking into the future, the prospects for improving these bounds are good. Indeed, as mentioned in Sec. 6 of [21], Virgo+ science run 4 (VSR4) was expected to be sensitive to fiducial ellipticities of a few $\times 10^{-4}$ for the Vela pulsar and $\sim 10^{-5}$ for the Crab pulsar and J1952+3252 if it achieved its sensitivity goal, and preliminary results using data from this run indeed give improved bounds for the Crab and Vela pulsars [25]. These improvements would bound the $l = m = 2$ surface deformation of the Vela pulsar to be below its rotational surface deformation for EOSs with larger radii, and place the bounds for the Crab pulsar and J1952+3252 well below their rotational surface deformation for all masses and EOSs. (Of course, in the most optimistic scenario, one would obtain a measurement of the $l = m = 2$ surface deformation instead of a bound.) There are also several other pulsars for which the Enhanced LIGO and Virgo+ observations already made could be able to beat the spindown limit (as discussed in Sec. 6 of [15]).

Advanced LIGO and Virgo are expected to have sensitivities more than 10 times better than the initial interferometers for the pulsars considered in [15], which would allow them to further improve the bounds on the pulsars already considered and to place bounds below the spin-down limit for many more pulsars (at least 47, based on the results in Sec. 2.2 of Pitkin [22]). And looking even further into the future, Pitkin [22] predicts that the Ein-

stein Telescope will place bounds below the spin-down limit for hundreds of pulsars. Additionally, as shown in Fig. 3 of Pitkin [22], the majority of the stars for which these detectors are expected to beat the spin-down limit have (relatively) small spin frequencies, so constraining the $l = m = 2$ surface deformation to be smaller than the expected $l = 2, m = 0$ rotational deformation gives another (vaguely physical) benchmark for searches, below the spin-down limit. However, we must stress once again that there is no expected relation between the two deformations.

On the theoretical side, it would be interesting to compute the rotational surface deformation of more rapidly rotating stars using either LORENE [41] or RNS [48] and compare with the slow-rotation predictions given here. Such a calculation, or the more involved calculations likely needed to obtain the bounds on the $l = m = 2$ surface deformations of more rapidly rotating stars from bounds on their gravitational wave emission, could be of interest in interpreting results from next-generation detectors, which are expected to be able to beat the spin-down limit (by a bit) for one or two pulsars with spin frequencies of ~ 500 Hz (see Fig. 3 in Pitkin [22]). However, these frequencies are still low enough (compared to the Kepler frequency) that our slow-rotation approximation is likely still reasonably accurate (within tens of percent). (See the values for the discrepancy in the quadrupole moment in matching a Hartle-Thorne slow-rotation solution to an exact numerical solution as a function of rotation parameter in Table 6 of Berti *et al.* [61], and the values for the Kepler frequency in, e.g., Fig. 2 of Lo and Lin [62].)

Likely more important would be the inclusion of the magnetic field in the calculation of the conversion from the $m = 2$ quadrupole moment to the surface deformation: As discussed in the Appendix, it is possible that small departures from a force-free configuration at the star's surface could affect the conversion for standard pulsar magnetic fields. And even if the magnetic field configuration is force-free to better accuracy than we need, the order-of-magnitude estimates of its effects on the computation given in Eq. (A.1) suggest that for magnetar-level surface magnetic fields of $\sim 10^{15}$ G, and the fiducial ellipticities of around 10^{-6} associated with internal fields of this magnitude (as given in, e.g., Sec. 7 of Friebe and Rezzolla [13]), the effects of the magnetic field could be large enough to affect the results we have given for the shape. However, it is worth noting that the internal field could be significantly larger than the surface field (as discussed in, e.g., Corsi and Owen [63]), in which case the corrections would be significantly smaller. Additionally, if the magnetic field is in the twisted torus configuration with a large toroidal component, then, as Ciolfi and Rezzolla [14] have very recently shown, the fiducial ellipticities can be considerably larger, $\sim 10^{-4}$, at least for a polytropic equation of state, which would also significantly reduce the correction.

Acknowledgments

We thank B. Brügmann, B. J. Owen, and the anonymous referee for useful comments. This work was supported by the DFG SFB/Transregio 7.

Appendix: Corrections due to non-perfect fluid contributions

Since we have obtained our results for the $l = m = 2$ shape deformation using expressions that were derived assuming an unmagnetized perfect fluid star, we need to check that they are still valid in the cases in which we are interested, where the star is perturbed not by the tidal field of a companion (as in Damour and Nagar [31]), but by some internal stresses. (Since we assume that we can treat these internal stresses as a first-order perturbation, we do not need to worry about their effects on the rotational deformation, since the two perturbations will be independent, to the order we are computing.) It turns out that we can indeed apply these expressions with no changes, if one assumes that the stresses at the star's surface (times R^2 or $1/\rho_-$) are much smaller than $H_0(R)$, which we shall see is the case in the majority of situations of interest. Explicitly, one needs to make this assumption in obtaining the expression for the star's perturbed surface using its enthalpy perturbation [see Eq. (26) in Damour and Nagar [31]], and also in writing the metric function $K(R)$ in terms of $H_0(R)$ and $H'_0(R)$ [see the discussion around Eq. (8)].

In the first case, the expression for the enthalpy used to obtain the position of the perturbed surface is obtained from stress-energy conservation. The relevant equation including the stress terms is given in Eq. (A2) of Ipser [33], and with slightly different notation in Eq. (35) of [10]. In the second case, Ipser gives the relation between K and H_0 including the stress terms in Eq. (39a).

We now consider the extent to which realistic surface stresses affect these results. Looking at the second case first, the star's magnetic field produces a stress of $\sim B^2/8\pi$, so the fractional corrections from these stresses to the relation between K and H_0 will be on the order of

$$\begin{aligned} &\sim \frac{B^2 R^2}{H_0(R)} = \frac{B^2 M^3 R^2}{\pi Q_{22} \bar{H}_0(R)} \\ &\simeq 10^{-9} \left(\frac{M}{1.4 M_\odot} \right)^3 \left(\frac{R}{10 \text{ km}} \right)^2 \left(\frac{B}{10^{12} \text{ G}} \right)^2 \left(\frac{10^{-4}}{\epsilon_{\text{fid}, 22}} \right). \end{aligned} \quad (\text{A.1})$$

[We have omitted the dependence on the star's compactness from $\bar{H}_0(R)$ in the final expressions here and later, though it will further suppress these corrections for higher-mass stars.]

Considering the corrections to the stress-energy conservation equation used to locate the star's surface, we have fractional corrections on the order of $R J^a F_{ab} / \rho_s H_0(R)$, since the addition to stress-energy conservation from the

electromagnetic field is $\nabla^b T_{ab}^{\text{EM}} = J^b F_{ab}$, where J^a and F_{ab} denote the (4-)current density and Faraday tensor, respectively. [Compare Eq. (35) in [10]; the magnetic field term would appear on the right-hand side of that equation, and the factor of R comes from the factor of $\nabla_a Y_{lm}$ that multiplies everything else in that expression.]

We expect $J^a F_{ab}$ (which gives the Lorentz force density) to be small, compared to ρ_s/R , since the magnetic field in the magnetosphere is expected to be close to force-free (as is discussed, e.g., at the end of Sec. 2.2 in [64]). If one takes the magnetosphere to be *exactly* force-free (as is frequently done in models of magnetically deformed neutron stars), then $J^a F_{ab}$ is zero. However, in the situations we consider, $J^a F_{ab}$ could be of the same order as the H_0 term, since in this case, the Lorentz force could help balance the gravitational perturbation, instead of the pressure perturbation alone balancing it, which is what occurs in the absence of additional stresses. But treating this properly is a task for far more detailed neutron star modeling (analogous to the issue with surface currents discussed in Sec. II C of Corsi and Owen [63]), so we simply take the magnetic field configuration to be exactly force-free here.

For the Crab pulsar, with a surface field of $\sim 4 \times 10^{12}$ G, one would have to consider a fiducial ellipticity of at most $\sim 10^{-11}$ for the first of these corrections to approach the percent level. This is well below the predicted sensitivity of even the proposed Einstein Telescope (see, e.g., Fig. 3 in Pitkin [22]), and around the minimum ellipticity quoted in [19] as being produced by an internal field of the same magnitude as the Crab's external field. (The Frieben and Rezzolla [13] fits predict an ellipticity of $\sim 10^{-9}$ for an internal field of that strength.) The other three pulsars considered in Table I have external magnetic fields of similar magnitudes [65], so this analysis holds for them, as well.

On the other hand, if we consider a solid strange quark star, the surface shear stresses could be quite large, if the gap parameter does not decrease too much as one approaches the star's surface and the high breaking strain assumed for the high-pressure interior continues to the surface—see the discussion in Sec. IV C of [10]. However, it seems likely that the stresses will be considerably smaller in any sort of reasonable case, since one expects both the gap parameter and breaking strain to decrease as the pressure decreases. And if one assumes that the

surface is not strained much more than the star's average strain, then the surface stress cannot be too large in the cases of interest.

Specifically, considering the KRV1 strange quark EOS, we have ratios of (in order of magnitude, and putting in the ~ 15.5 km radius appropriate for a $1.4 M_\odot$ star with this EOS, in addition to the associated values of the Mannarelli, Rajagopal, and Sharma [53] shear modulus)

$$\begin{aligned} &\sim \frac{\mu_- \sigma_- R^2}{H_0(R)} = \frac{M^3 \mu_- \sigma_- R^2}{\pi Q_{22} \bar{H}_0(R)} \\ &\simeq 10^{-3} \left(\frac{M}{1.4 M_\odot} \right)^3 \left(\frac{R}{15.5 \text{ km}} \right)^2 \left(\frac{\mu_-}{10^{33} \text{ erg cm}^{-3}} \right) \\ &\quad \times \left(\frac{\sigma_-}{\epsilon_{\text{fid}, 22}} \right), \end{aligned} \tag{A.2}$$

and

$$\begin{aligned} &\sim \frac{\mu_- \sigma_-}{H_0(R) \rho_-} = \frac{M^3 \mu_- \sigma_-}{\pi Q_{22} \bar{H}_0(R) \rho_-} \\ &\simeq 10^{-1} \left(\frac{M}{1.4 M_\odot} \right)^3 \left(\frac{\mu_- / \rho_-}{10^{-2}} \right) \left(\frac{\sigma_-}{\epsilon_{\text{fid}, 22}} \right), \end{aligned} \tag{A.3}$$

where $\mu_- \sigma_-$ is the shear stress just inside the star's surface (written as a product of shear modulus μ_- and shear strain σ_-). (These come, as before, from the corrections to the relation between K and H_0 and to the enthalpy expression used to locate the star's surface.)

While it is possible that σ_- could be as large as $\sim 10^{-1}$, around the breaking strain for the neutron star outer crust obtained in [54, 55] (and thus orders of magnitude larger than $\epsilon_{\text{fid}, 22}$ for the stars we are considering), this high breaking strain comes from high pressure, so the breaking strain at the surface, where the pressure goes to zero, will likely be much less. Moreover, if one assumes that the star's surface is strained at about the same level as the star's average strain, then we will have $\sigma_- \simeq \epsilon_{\text{fid}, 22}$ (cf. Fig. 10 in [10], remembering that one can linearly scale the maximum quadrupoles given there for a uniform strain of 10^{-1} to any uniform strain). Thus, we feel comfortable quoting values for the strange quark star case, since the caveats seem fairly mild in reasonable situations.

[1] L. Lindblom and A. K. M. Masood-ul-Alam, Commun. Math. Phys. **162**, 123 (1994).
[2] A. K. M. Masood-ul-Alam, Gen. Relativ. Gravit. **39**, 55 (2007).
[3] L. Lindblom, Phil. Trans. R. Soc. A **340**, 353 (1992).
[4] <http://echo.jpl.nasa.gov>.
[5] M. W. Busch, Ph.D. thesis, The California Institute of Technology (2010).
[6] N. K. Pavlis, S. A. Holmes, S. C. Kenyon, and

J. K. Factor, J. Geophys. Res. **117**, B04406 (2012), URL http://earth-info.nga.mil/GandG/wgs84/gravitymod/egm2008/egm2008_060.txt.
[7] M. Ruderman, Nature (London) **223**, 597 (1969).
[8] S. Chandrasekhar and E. Fermi, Astrophys. J. **118**, 116 (1953), **122**, 208(E) (1955).
[9] B. J. Owen, Phys. Rev. Lett. **95**, 211101 (2005).
[10] N. K. Johnson-McDaniel and B. J. Owen, arXiv:1208.5227 [astro-ph.SR].
[11] R. Ciolfi, V. Ferrari, and L. Gualtieri, Mon. Not. R. As-

- tron. Soc. **406**, 2540 (2010).
- [12] S. Yoshida, K. Kiuchi, and M. Shibata, *Phys. Rev. D* **86**, 044012 (2012).
- [13] J. Frieben and L. Rezzolla, *Mon. Not. R. Astron. Soc.* **427**, 3406 (2012).
- [14] R. Ciolfi and L. Rezzolla, arXiv:1306.2803 [astro-ph.SR].
- [15] B. P. Abbott *et al.* (LIGO Scientific Collaboration and Virgo Collaboration), *Astrophys. J.* **713**, 671 (2010).
- [16] B. J. Owen, *Classical Quantum Gravity* **26**, 204014 (2009).
- [17] B. Abbott *et al.* (LIGO Scientific Collaboration), *Phys. Rev. D* **76**, 042001 (2007).
- [18] C. Palomba, *Astron. Astrophys.* **354**, 163 (2000).
- [19] B. Abbott *et al.* (LIGO Scientific Collaboration), *Astrophys. J. Lett.* **683**, L45 (2008), **706**, L203(E) (2009).
- [20] J. Abadie *et al.* (LIGO Scientific Collaboration), *Astrophys. J.* **722**, 1504 (2010).
- [21] J. Abadie *et al.* (LIGO Scientific Collaboration and Virgo Collaboration), *Astrophys. J.* **737**, 93 (2011).
- [22] M. Pitkin, *Mon. Not. R. Astron. Soc.* **415**, 1849 (2011).
- [23] P. Astone (for the LIGO Scientific Collaboration and Virgo Collaboration), *Classical Quantum Gravity* **29**, 124011 (2012).
- [24] D. I. Jones, *Mon. Not. R. Astron. Soc.* **402**, 2503 (2010).
- [25] C. D. Gill, Ph.D. thesis, The University of Glasgow (2012).
- [26] S. Taylor and E. Poisson, *Phys. Rev. D* **78**, 084016 (2008).
- [27] P. Anninos, D. Bernstein, S. R. Brandt, D. Hobill, E. Seidel, and L. Smarr, *Phys. Rev. D* **50**, 3801 (1994).
- [28] S. R. Brandt and E. Seidel, *Phys. Rev. D* **52**, 870 (1995).
- [29] S. Brandt, K. Camarda, E. Seidel, and R. Takahashi, *Classical Quantum Gravity* **20**, 1 (2003).
- [30] T. Regge and J. A. Wheeler, *Phys. Rev.* **108**, 1063 (1957).
- [31] T. Damour and A. Nagar, *Phys. Rev. D* **80**, 084035 (2009).
- [32] T. Hinderer, *Astrophys. J.* **677**, 1216 (2008), **697**, 964(E) (2009).
- [33] J. R. Ipser, *Astrophys. J.* **166**, 175 (1971).
- [34] K. S. Thorne, *Rev. Mod. Phys.* **52**, 299 (1980).
- [35] J. B. Hartle, *Astrophys. J.* **150**, 1005 (1967).
- [36] K. S. Thorne and A. Campolattaro, *Astrophys. J.* **149**, 591 (1967), **152**, 673(E) (1968).
- [37] J. B. Hartle and K. S. Thorne, *Astrophys. J.* **153**, 807 (1968).
- [38] L. Lindblom, *Astrophys. J.* **398**, 569 (1992).
- [39] K. H. Lockitch, Ph.D. thesis, The University of Wisconsin-Milwaukee (1999).
- [40] J. S. Read, B. D. Lackey, B. J. Owen, and J. L. Friedman, *Phys. Rev. D* **79**, 124032 (2009).
- [41] <http://www.lorene.obspm.fr>.
- [42] P. B. Demorest, T. Pennucci, S. M. Ransom, M. S. E. Roberts, and J. W. T. Hessels, *Nature (London)* **467**, 1081 (2010).
- [43] A. Akmal, V. R. Pandharipande, and D. G. Ravenhall, *Phys. Rev. C* **58**, 1804 (1998).
- [44] M. Baldo, I. Bombaci, and G. F. Burgio, *Astron. Astrophys.* **328**, 274 (1997).
- [45] F. Douchin and P. Haensel, *Astron. Astrophys.* **380**, 151 (2001).
- [46] N. K. Glendenning, *Astrophys. J.* **293**, 470 (1985).
- [47] R. B. Wiringa, V. Fiks, and A. Fabrocini, *Phys. Rev. C* **38**, 1010 (1988).
- [48] <http://www.gravity.phys.uwm.edu/rns/>.
- [49] N. K. Johnson-McDaniel and B. J. Owen, *Phys. Rev. D* **86**, 063006 (2012), **87**, 129903(E) (2013).
- [50] A. Kurkela, P. Romatschke, and A. Vuorinen, *Phys. Rev. D* **81**, 105021 (2010).
- [51] J. Antoniadis *et al.*, *Science* **340**, 1233232 (2013).
- [52] C. J. Horowitz, *Phys. Rev. D* **81**, 103001 (2010).
- [53] M. Mannarelli, K. Rajagopal, and R. Sharma, *Phys. Rev. D* **76**, 074026 (2007).
- [54] C. J. Horowitz and K. Kadau, *Phys. Rev. Lett.* **102**, 191102 (2009).
- [55] K. Hoffman and J. Heyl, *Mon. Not. R. Astron. Soc.* **426**, 2404 (2012).
- [56] A. G. Lyne, R. S. Pritchard, and F. Graham-Smith, *Mon. Not. R. Astron. Soc.* **265**, 1003 (1993), URL <http://www.jb.man.ac.uk/~pulsar/crab.html>.
- [57] M. Bejger, *Astron. Astrophys.* **552**, A59 (2013).
- [58] J. P. W. Verbiest, J. M. Weisberg, A. A. Chael, K. J. Lee, and D. R. Lorimer, *Astrophys. J.* **755**, 39 (2012).
- [59] A. W. Steiner, J. M. Lattimer, and E. F. Brown, *Astrophys. J.* **722**, 33 (2010).
- [60] A. W. Steiner, J. M. Lattimer, and E. F. Brown, *Astrophys. J. Lett.* **765**, L5 (2013).
- [61] E. Berti, F. White, A. Maniopoulou, and M. Bruni, *Mon. Not. R. Astron. Soc.* **358**, 923 (2005).
- [62] K.-W. Lo and L.-M. Lin, *Astrophys. J.* **728**, 12 (2011).
- [63] A. Corsi and B. J. Owen, *Phys. Rev. D* **83**, 104014 (2011).
- [64] A. Colaiuda, V. Ferrari, L. Gualtieri, and J. A. Pons, *Mon. Not. R. Astron. Soc.* **385**, 2080 (2008).
- [65] R. N. Manchester, G. B. Hobbs, A. Teoh, and M. Hobbs, *Astron. J.* **129**, 1993 (2005), URL <http://www.atnf.csiro.au/people/pulsar/psrcat/>.